Supporting Information

Expanding the Upper Limits of Robustness of Cellulose Nanocrystal Aerogels: Outstanding Mechanical Performance and Associated Pore Compression of Chiral-Nematic Architectures

Anurodh Tripathi[a,b,±], Blaise L. Tardy[b,±,*], Saad A. Khan[a], Falk Liebner[c], Orlando J. Rojas[a,b,*]

[a]Department of Chemical & Biomolecular Engineering, NC State University, Raleigh, NC 27695-7905, USA.
[b]Department of Byproducts and Biosystems, School of Chemical Engineering, Aalto University, P.O. Box 16300, FIN-00076 Aalto, Espoo, Finland.
[c]Division of Chemistry of Renewable Resources, University of Natural Resources and Life Sciences, Konrad-Lorenz-Straße 24, 3430 Tulln, Austria
[±] These authors contributed equally

Table S1: Characteristics associated with gel formation.

Initial CNC conc. (wt %)	Anisotropic volume fraction	Gel fraction	Gel Volume Shrinkage (%)	Final conc. after gelation (wt%)
4	0.22	0.41	59	12.4
5.5	0.59	0.59	41	14.8
7	1	0.59	41	17.2

Table S2: Mechanical properties of the CN-CNC aerogels

Samples	Density ($g.cm^{-3}$)	Modulus (MPa)	Densification strain (%)	Specific modulus ($MPa.cm^3.g^{-1}$)	Specific toughness ($MJ.m^{-3}.g^{-1}.cm^3$)	Specific strength ($MPa.cm^3.g^{-1}$)
AG-4	0.137	0.17	80	1.24	0.98	5.18
AG-5.5	0.156	0.45	67	2.89	2.59	15.38
AG-7	0.199	1.9	64	9.55	2.99	17.59
EISA-10	0.171	1.7	52	9.94	3.55	21.52
EISA-20	0.329	1.6	48	4.86	3.04	15.74
EISA-25	0.428	2.5	30	5.84	N.A.	N.A.

**The toughness was measured until 70% strain and strength were measured at 70 % strain. For EISA-25, such high strain was not achieved.

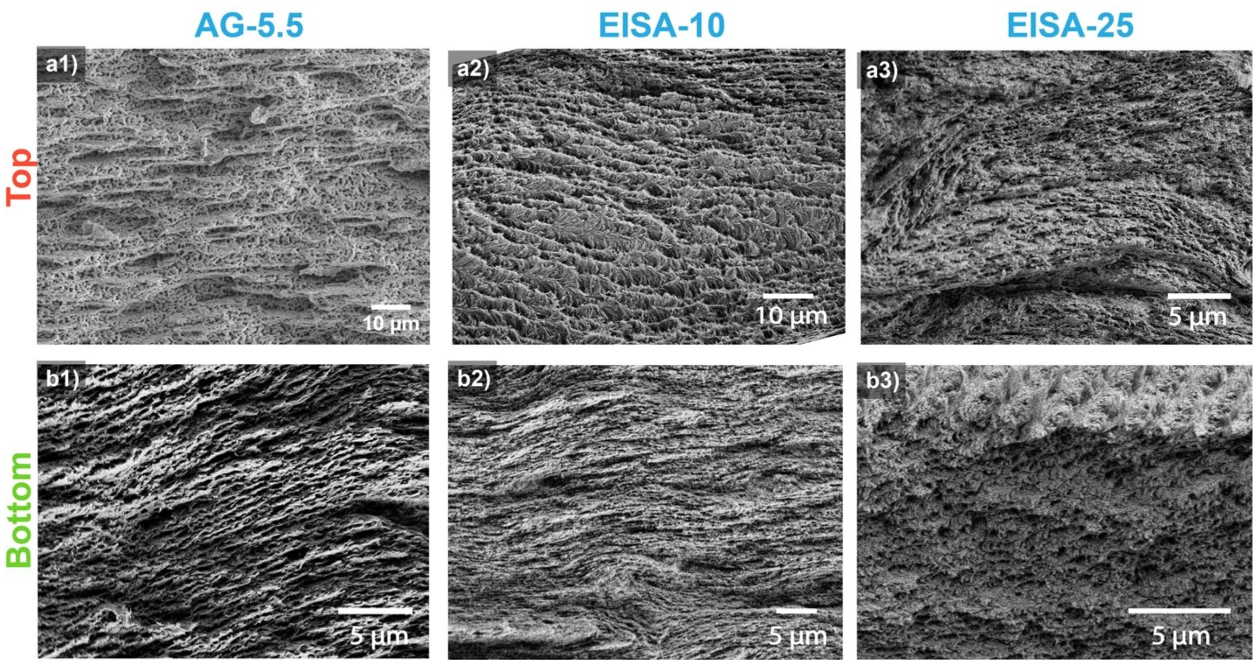

Figure S1: SEM images of the aerogels cross-section observed perpendicular to the principal plane of the assembly, across chiral-nematic pitches. Top row exhibits image near the top cross-section, a1) AG-5.5, a2) EISA-10, a3) EISA-25. Bottom row exhibits images near the bottom cross- section, b1) AG-5.5, b2) EISA-10, and, b3) EISA-25. In the top of panel b3 a Bouligand cut can be observed further highlighting the chiral nematic order.

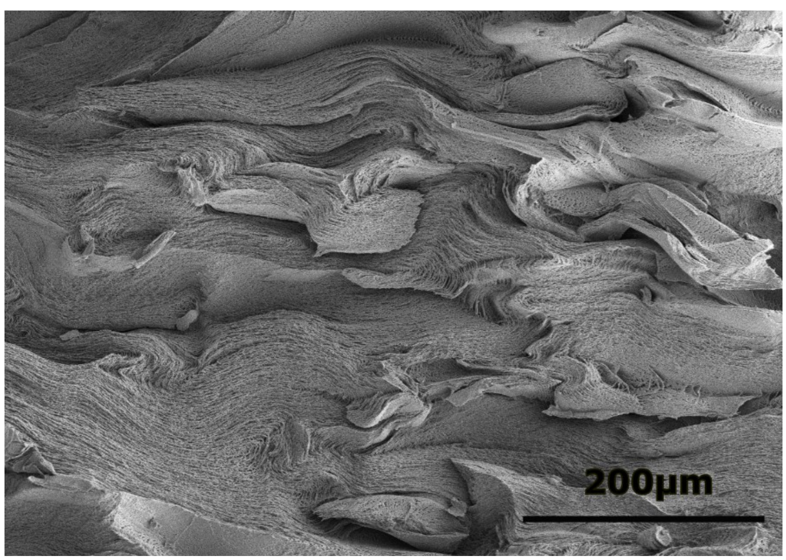

Figure S2: The bottom cross-section of the AG-4 aerogel

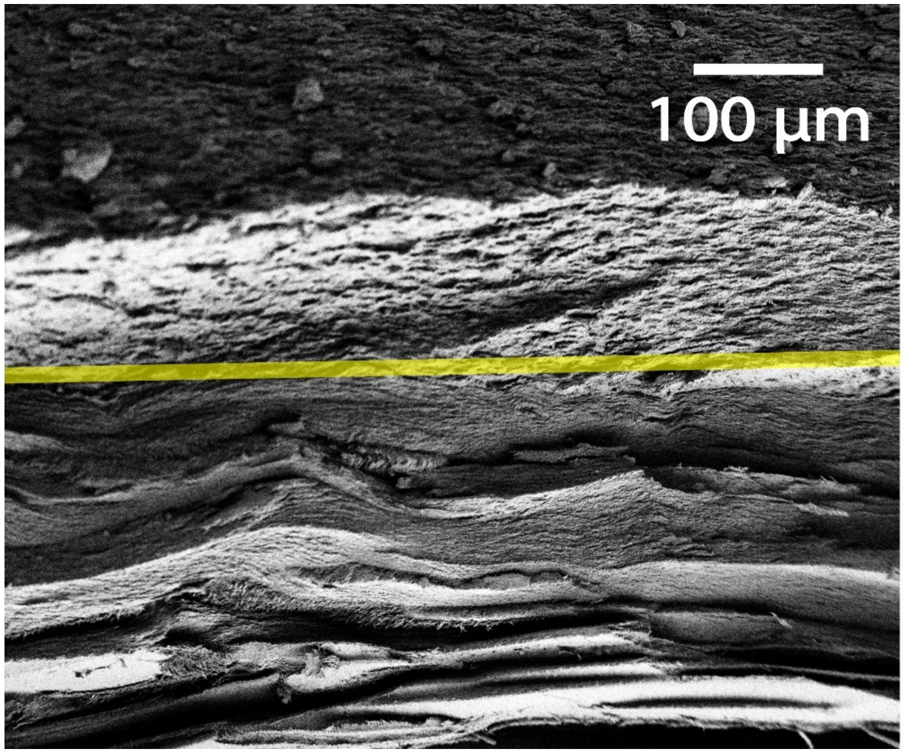

Figure S3: Transition from isotropically ordered (above yellow line) to anisotropically ordered (below yellow line) AG-7.

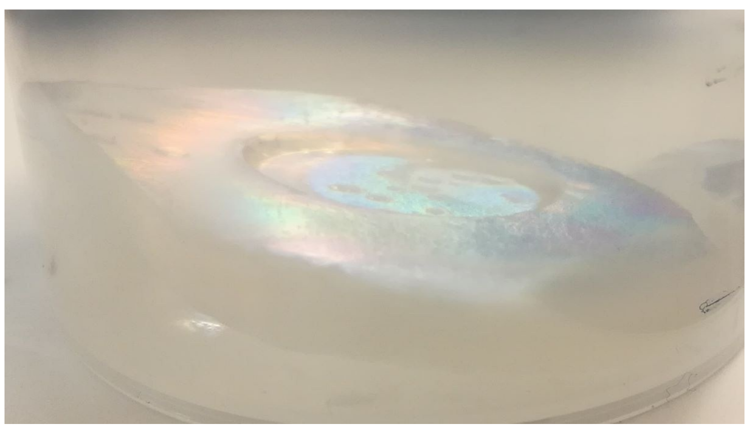

Figure S4: The bottom surface of the EISA-20 gel exhibiting iridescence.

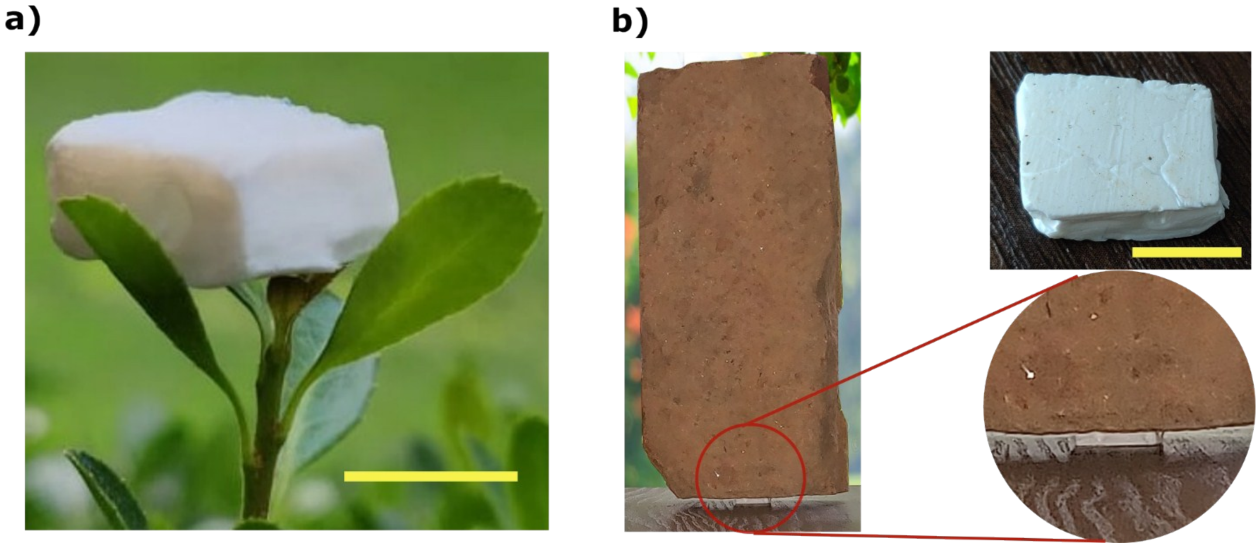

Figure S5: A physical demonstration of lightness and toughness of CNC aerogel. a) The AG-5.5 aerogel on the surface of a leaf, b) Same AG-5.5 aerogel underneath a 2 Kg brick. The inset shows the unbroken aerogel after the brick was removed. The scale bars are 1 cm.

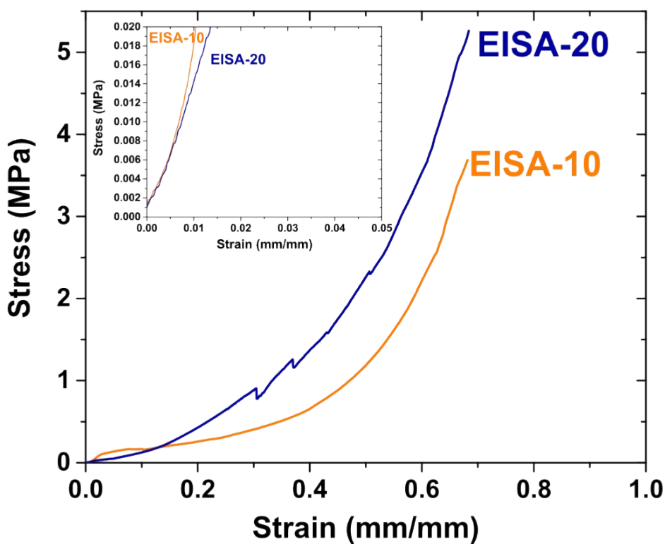

Figure S6: The compressive stress-strain curves for EISA-10 and 20 samples. The inset shows magnification of the curve at low strains.

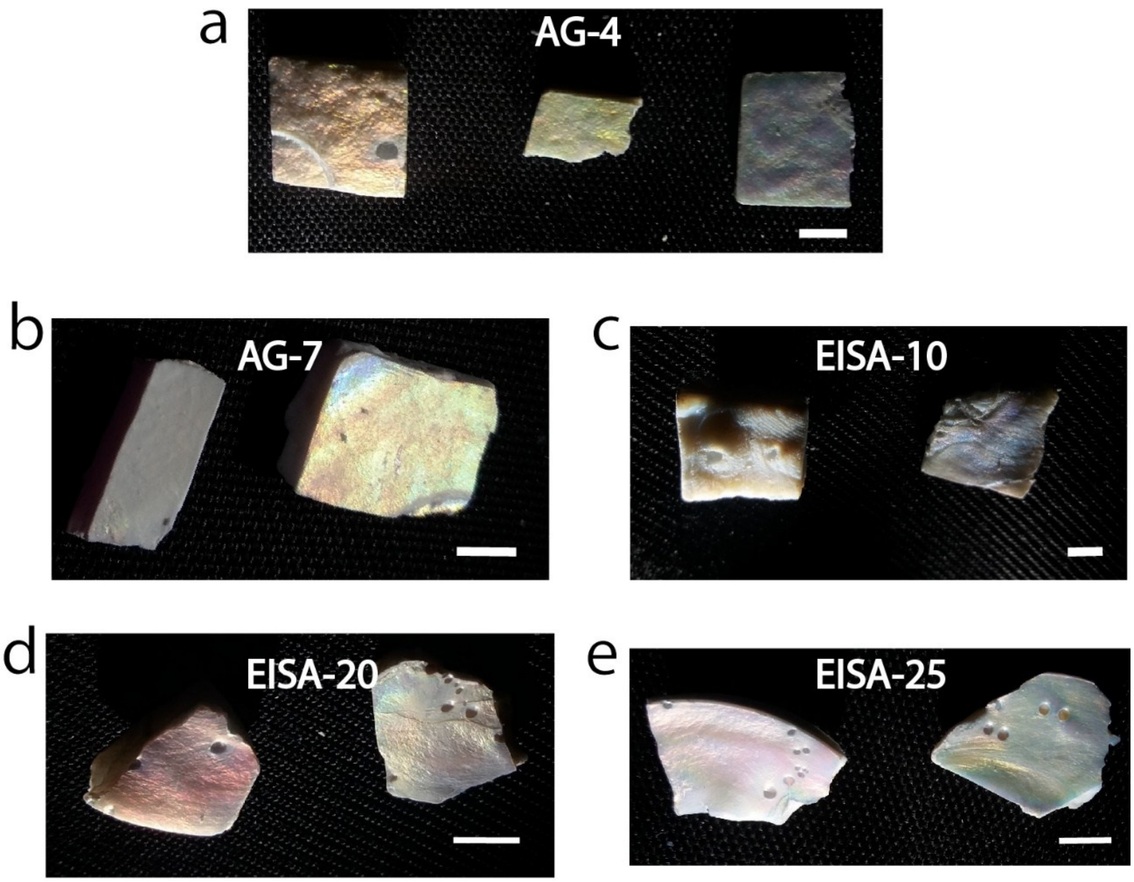

Figure S7: Photographic images of aerogels prior (left in each panel) and after compression (right in each panel) for a) AG-4, b) AG-7, c) EISA-10, d) EISA-20. and e) EISA-25. The shift to lower wavelength reflections highlight compression of the chiral nematic pitch to smaller pitches. In a) the central aerogel is a fragment of the patially compressed AG-4 as reported in Table 1. Scale bar is 5 mm.

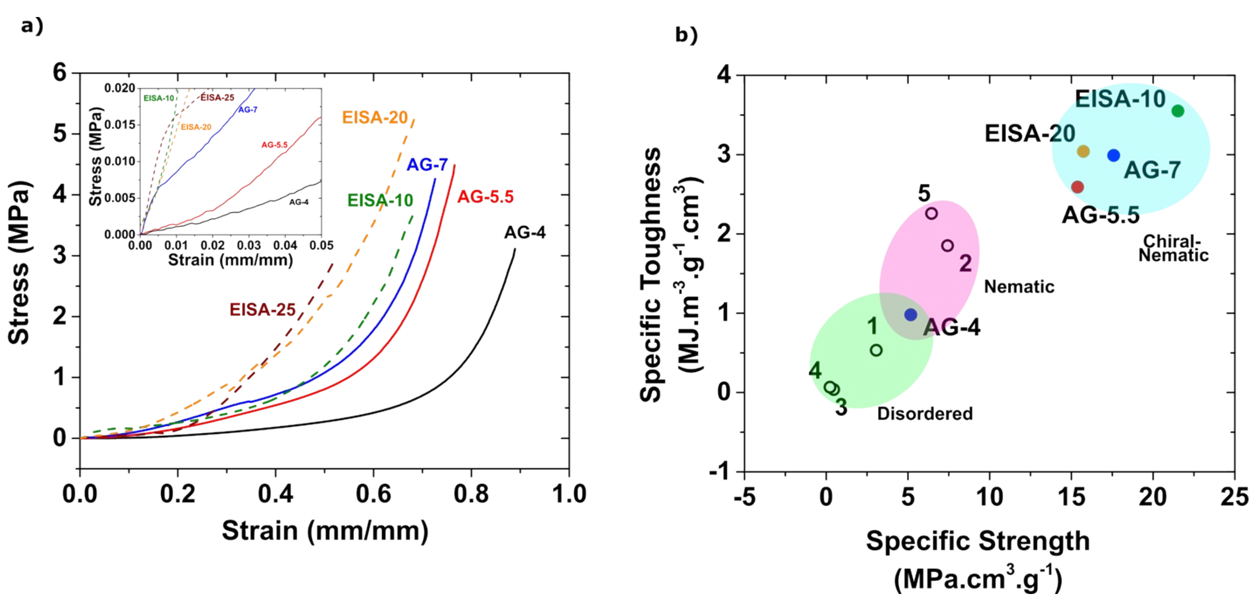

Figure S8: A plot of specific toughness vs specific strength exhibiting the mechanical properties obtained for CNC aerogels in this study (closed circle) compared to previously reported in the literature (open circle). References from the manuscript: 1: Abraham et al.[40], 2: Plappert et al.[21], 3: Yang & Cranston[41], 4: Yang et al.[42], 5: Kobayashi et al.[27].

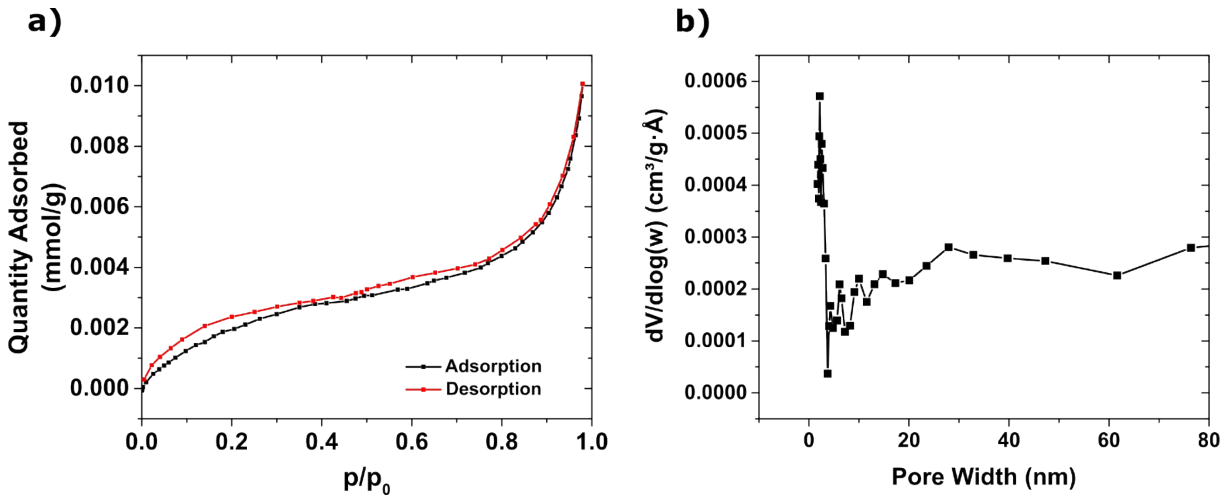

Figure S9: a) The N_2 adsorption, and b) PSD curve for the CNC films prepared by EISA. A 500 mg sample was used, 5 times more as used for the EISA aerogel samples. The BET area was calculated as 0.2 m^2/g.